Supporting Information

Palladium structure engineering induced by electrochemical H intercalation boosts hydrogen evolution catalysis

Guangxia Wang,[a] Jinyang Liu,[a] Yongming Sui,*[a] Ming Wang,[b] Liang Qiao,*[b] Fei Du,[c] and Bo Zou*[a]

[a]State Key Laboratory of Superhard Materials, Jilin University, Changchun 130012, China. Email: zoubo@jlu.edu.cn; suiym@jlu.edu.cn

[b]Department of Materials Science and Engineering, College of Science, Changchun University, Changchun 130012, China

[c]Laboratory of Physics and Technology for Advanced Batteries (Ministry of Education), College of Physics, Jilin University, Changchun 130012, China.

Experimental Section

Chemical and materials: Na_2PdCl_4, (99.99%), PVP (Mw ≈ 55,000), ascorbic acid, KBr, Ethylene glycol (EG) were purchased from Sigma-Aldrich. HCl (36.5-38.0%), acetone were purchased from Sinopharm Chemical Reagent Company. Deionized water (18.2MΩ·cm). All the chemicals and materials were used as received.

Synthesis of Pd icosahedron: The Pd icosahedron with an average size of ~14 nm were prepared according to the previous report with slight modification.[1] 30 mg of PVP was mixed with 2 mL of EG and the solution was preheated to 160 °C in an oil bath under a magnetic stirring. After 10 min, 1 mL of EG solution containing 8.9 mg of Na_2PdCl_4 and 16.7 μL of HCl was injected into the pre-heated solution. 35 μL of HCl was subsequently added to the reaction mixture. The vial was capped and kept at 160 °C for additional 10 min.

Synthesis of Pd nanocube: The Pd cube with an average edge length of 14 nm was prepared using a previously reported protocol.[2] For the synthesis of Pd Cube, 105 mg of PVP, 60 mg of AA, 400 mg of KBr were dissolved in 8.0 mL of deionized water. The mixture solution was heated at 80 °C under magnetic stirring for 10 min. After that, 3 mL of deionized water containing 57 mg of Na_2PdCl_4 was injected into the preheated solution. The vial was capped and kept at 80 °C for 3 h.

***Synthesis of Pd octahedron*:** The Pd octahedron with an average size of 14 nm were prepared according to the previous report.[2] In a typical synthesis, 105 mg of PVP, 100 μL of HCHO, and 0.2 mL aqueous solution of Pd cube with an average edge length of 6 nm were dispersed in 8 mL of deionized water. The mixture was preheated to 60 °C for 5 min. Then, 3 mL of an aqueous solution containing 20 mg of Na_2PdCl_4 was quickly injected into the preheated solution and the reaction was kept at 60 °C for 3 h.

The products of Pd with different morphologies were collected by centrifugation, washed with deionized water and acetone for two times, and finally dried at 50 °C for 5 h for further use.

Synthesis of PdH_x icosahedron: The as-prepared Pd icosahedron was dispersed in DMF solution with the vial capped, which was kept at 160 °C for 16 h in an oil bath under a magnetic stirring. After cooling to room temperature, washed the products twice with water and ethanol.[3]

Preparation of the working electrode. First, carbon support (Cabot, Vulcan XC-72) and Pd nanocrystals (20 wt%) were respectively dispersed in ethanol and treated with ultrasound for 1 h. Then, the as-prepared Pd nanocrystal suspension was dispersed into carbon suppor dropwise. This mixture was continued to sonicate for 1 h and stirred for 6 h. After that, the resultant was precipitated out by centrifugation. After drying, 2.5 mg carbon-supported Pd nanocrystals were dispersed in a mixture of 800 μL of deionized water, 200 μL of isopropanol and 20 μL 5% wt Nafion. The mixture was treated with ultrasonication for 1 h. 4 μL of the suspension was deposited on a pre-cleaned glassy-carbon electrode with a diameter of 3 mm (the carbon supported catalyst loading mass is 0.142 $mg \cdot cm^{-2}$) and dried at ambient condition.

Commercial Pt/C was tested with same loading mass.

Electrochemical measurement. The electrochemical measurements were carried out by a three-electrode cell using a CHI660E electrochemical work station (Chenhua, China) at 20 °C. The three-electrode system consists of a glassy-carbon electrode (area, 0.07 cm^2) as the working electrode, a saturated calomel electrode as the reference electrode, and a 1 cm^2 platinum net as

the counter electrode. The working electrode and counter electrode were placed in different compartments separated by Nafion member to prevent Pt atoms from contaminating the working electrode.[4]

Linear sweep voltammetry (LSV) was conducted to test the HER activity from 0.3 V to -0.45 V (vs. RHE) with scan rate of 10 mV s^{-1} in 0.5 M H_2SO_4 solution. The stability was evaluated by the cyclic voltammogram (CV) cycling operated in 0.5 M H_2SO_4 solution from 0.2 V to -0.45 V (vs. RHE) at 100 mV s^{-1} test for designated cycles. The CV and LSV tests were conducted from 0.3 to -0.7 V at a respective rate of 100 and 10 mV s^{-1} in 0.1 M KOH. As for comparison, to avoid the falling of catalyst from the electrode caused by the large current density, we conducted the CV cycling and LSV of commercial Pt/C within 0.15 V and -0.15 V. Electrochemical impedance spectra (EIS) measurements were performed at a bias potential of -3 mV versus RHE with the frequency in the range of 0.1 Hz and 100, 000 Hz with the amplitude potential of 5 mV.[4,5]

ECSA is used to quantitatively evaluate surface area of exposure. The ESCAs of Pd and commercial Pt/C catalysts were calculated by cyclic voltammetry (CV) method. The scan region was from 0.05 V to 1.25 V vs. RHE at a sweep rate of 100 $mV \cdot s^{-1}$. A typical pair of peaks located around 0-0.3 V can be attributed to the adsorption and desorption of hydrogen. ECSA of Pd was calculated from the hydrogen desorption region and Pt was obtained from the hydrogen absorption.[6,7] ECSAs was calculated from the CV curves according to the following equation:

$$ECSA = Q/C \cdot m$$

Where Q is the charge from the hydrogen desorption peak area, C is the hydrogen adsorption constant (for Pd, C = 4.2 C m^{-2}; for Pt, C = 2.1 C m^{-2}) and m is the mass of the catalyst.

Characterizations. Transmission electron microscopy (TEM) and High-resolution transmission electron microscopy (HRTEM) images of the obtained samples were obtained on JEM 2200FS with an accelerating voltage of 200 kV. X-ray diffraction was tested on Rigaku with a high-

intensity microfocus rotating anode X-ray generator of MicroMax-007HF (λ=1.5418 Å). Angle-dispersive XRD experiments with a wavelength of 0.6199 Å beam were carried out in Beijing Synchrotron Radiation Facility. CeO_2 was used as the standard sample for calibration. The collected 2D images were integrated and analyzed using the FIT2D program to gain plots of intensity versus 2θ.

Computational methods

All the first-principles calculations are performed using density-functional theory (DFT) as implemented in CASTEP code.[8] The generalized gradient approximation (GGA) with Perdew-Burke-Ernzerhof (PBE) functional is used to treat the exchange-correlation potential.[9] The Vanderbilt ultrasoft pseudopotential and plane wave basis set with a cutoff energy of 500 eV are employed.[10] The Brillouin zone is sampled using 6×6×1 Monkhorst-Pack grid for Pd and PdH_x (111) surface.[11] The convergence tolerance of energy is 10^{-6} eV per atom. The DFT-D approach with the Tkatchenko-Scheffler (TS) scheme for dispersion correction is adopted.[12]

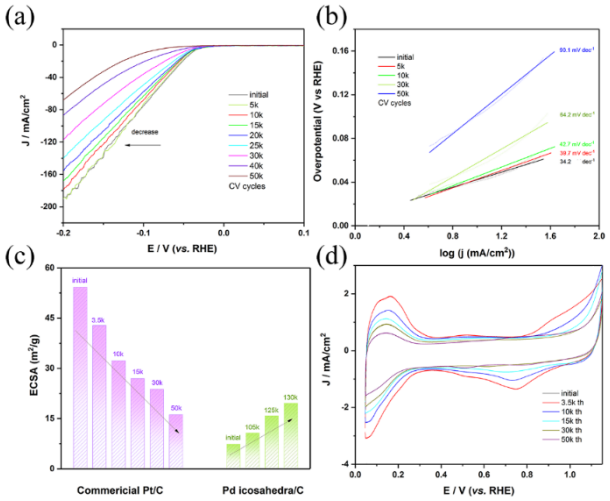

Figure S1 (a) Polarization curves, and (b) The corresponding Tafel plots of commercial Pt/C. (c) summerized ECSAs of commercial Pt/C and Pd icosahedron in 0.5 M H_2SO_4 at a scan rate of 100 mV s^{-1}.(d) CV curves of commercial Pt/C.

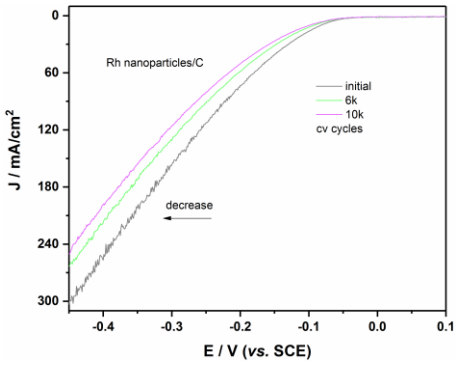

Figure S2 Polarization curves of Rh nanoparticles/C in 0.5 M H_2SO_4 at a scan rate of 10 mV s^{-1}.

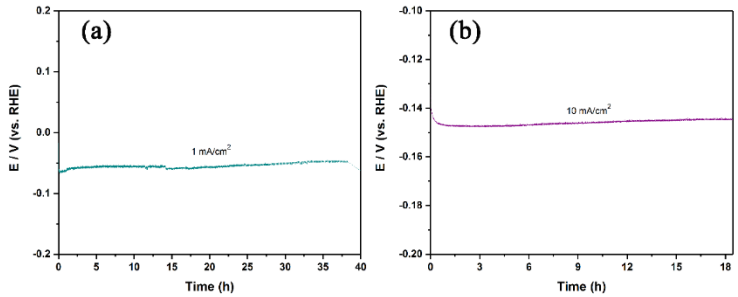

Figure S3 (a) i-t curves of Pd icosahedron at a current density of 1 mA cm^{-2}. (b) i-t curves of the same electrode worked at 10 mA cm^{-2} after cycling at 1 mA cm^{-2}.

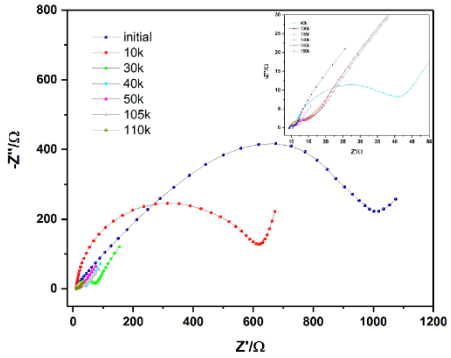

Figure S4 EIS of Pd icosahedron electrode after corresponding tests at 3 mV vs RHE.

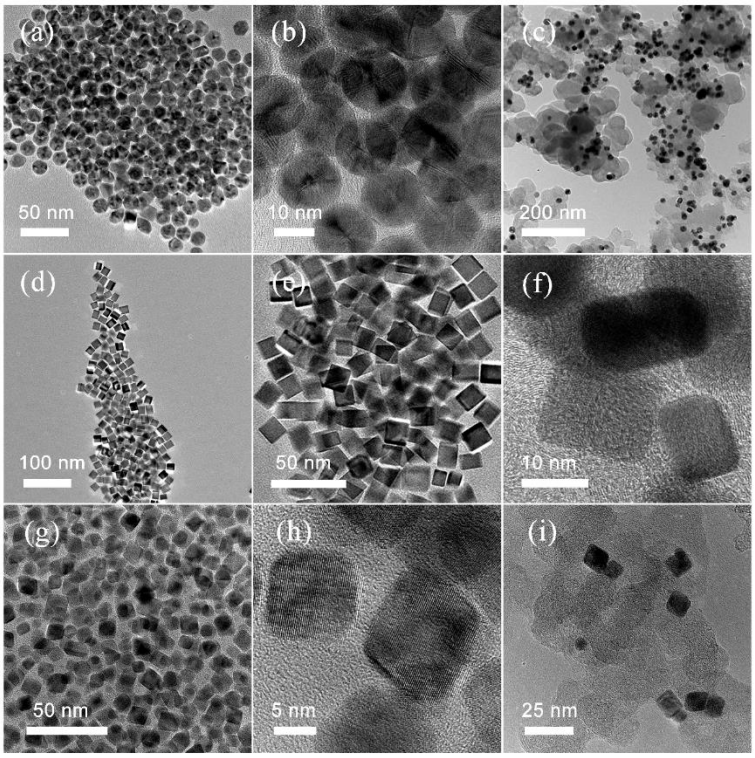

Figure S5 The First and second columns were low- and high-magnification TEM images of Pd nanoparticle with different morphologies, respectively. The third column was the electrode materials of Pd nanoparticles supported by C. (a-c) Pd icosahedron. (d-f) Pd cube. (g-i) Pd octahedron.

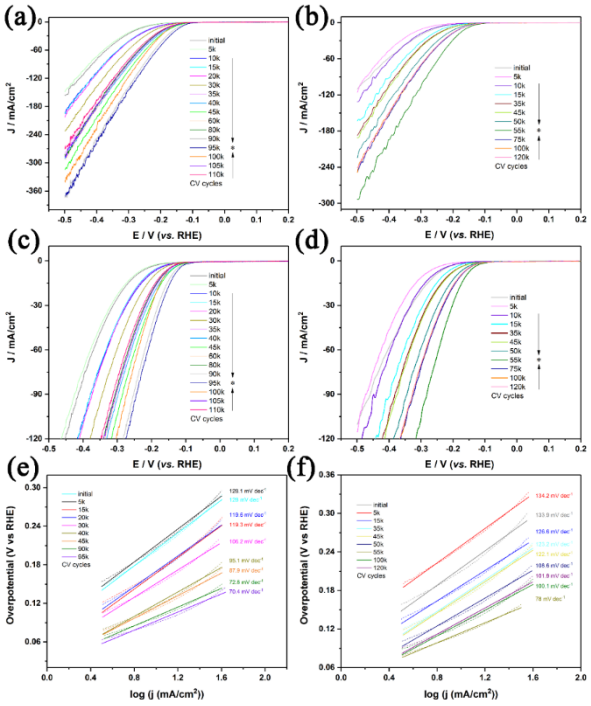

Figure S6 (a, c) Polarization curves, and (e) Tafel plots of Pd cube/C. (b, d) Polarization curves, and (f) Tafel plots of Pd octahedron/C.

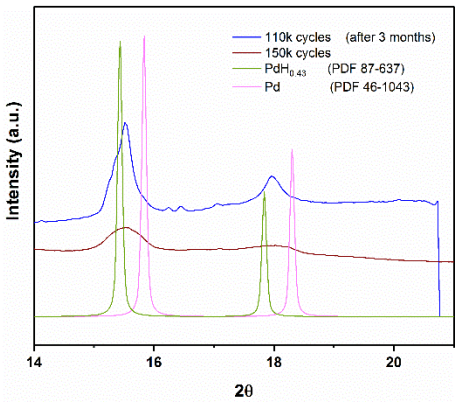

Figure S7 The ADXRD and XRD characterizations of Pd icosahedron /C after cycling 110,000 cycles and 150,000 cycles, repectively.

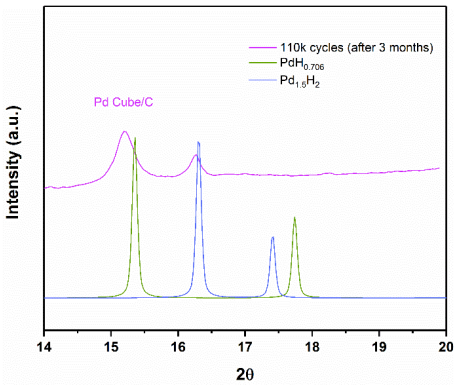

Figure S8 The ADXRD characterization of Pd cube /C cycling for 110,000 cycles after 3 months.

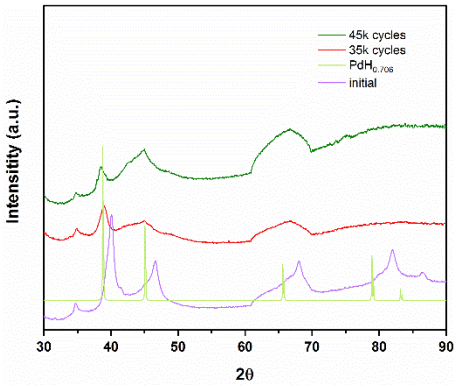

Figure S9 The XRD characterization of Pd octahedron /C cycling different cycles.

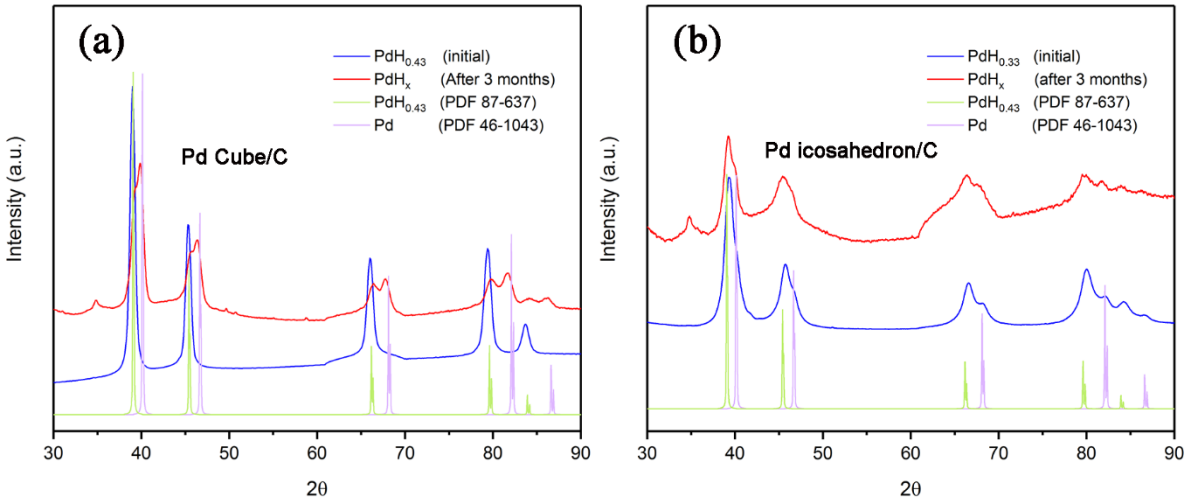

Figure S10 The stability of PdH_x prepared with DMF after 3 months under ambient conditions.

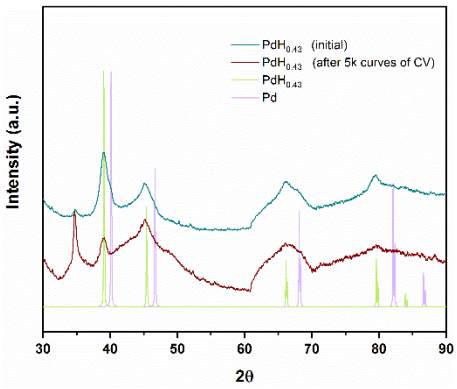

Figure S11 XRD patterns of $PdH_{0.43}$ icosahedron/C before and after 5,000 cycles of CV in 0.5 M H_2SO_4 between -0.2 and 0.9 V (vs SCE) with scan rate of 100 mV/s.

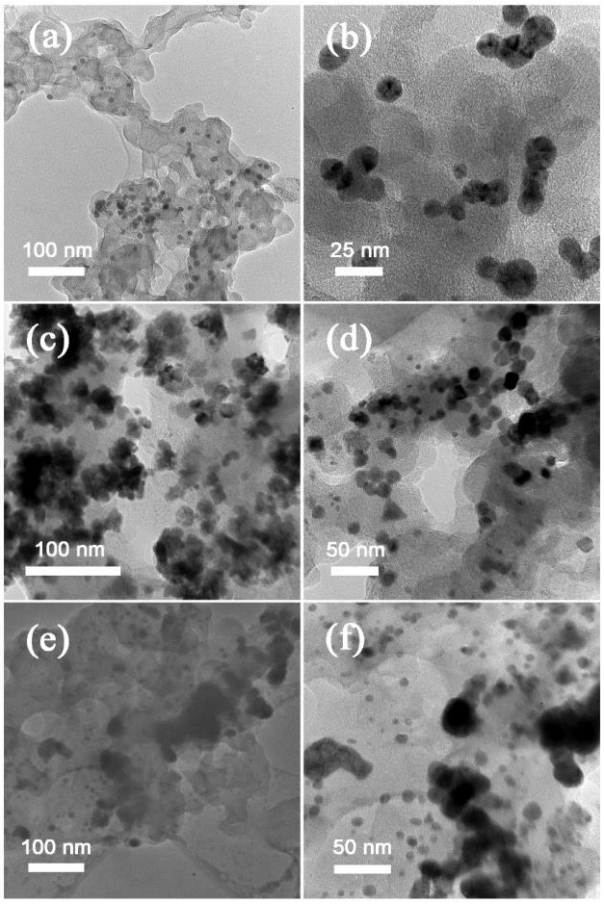

Figure S12 TEM images of (a, b) Pd icosahedron/C after cycling 150,000 cycles, (c ,d) Pd cube/C after 110,000 cycles and (e-f) Pd octahedra/C after 120,000 cycles.

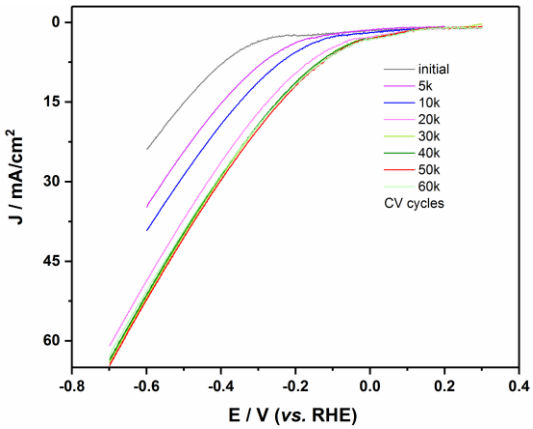

Figure S13 Polariztion curves of Pd icosahedron/C in 0.1 M KOH.

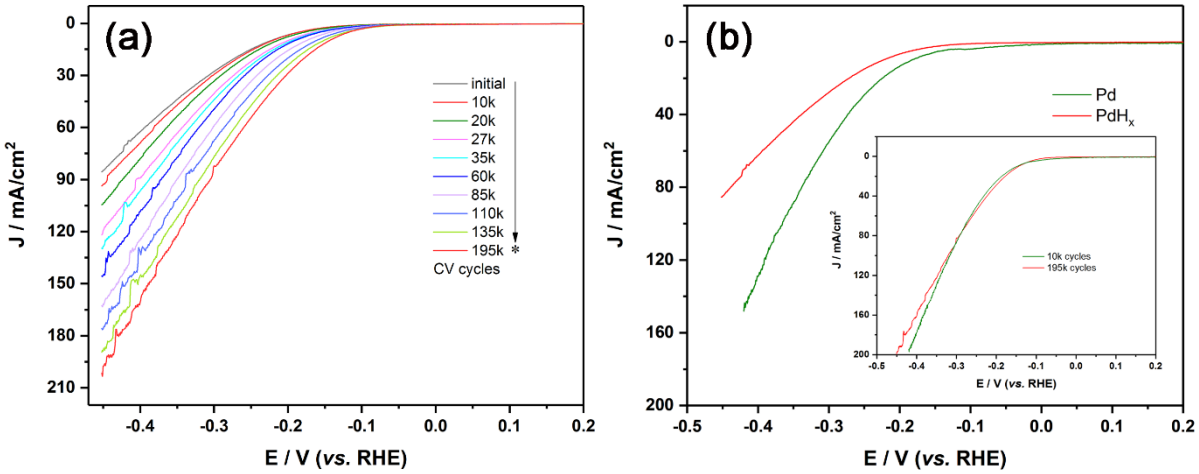

Figure S14 (a) Polarization curves of PdH_x icosahedron/C prepared with thermal DMF treatment. (b) The activities comparison of PdH_x icosahedron/C and Pd icosahedron/C. (x is approaximately 0.33)

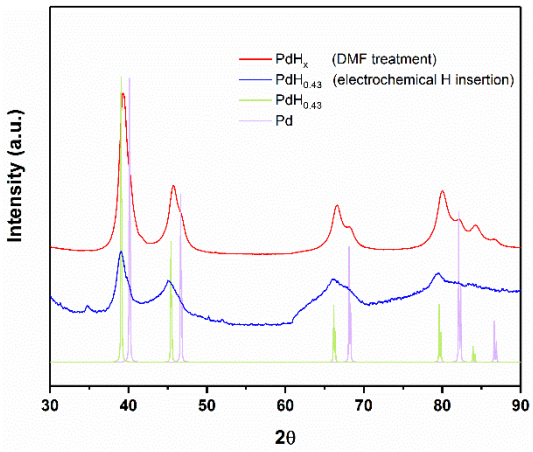

Figure S15 XRD patterns of PdH_x icosahedron/C prepared with thermal DMF treatment and $PdH_{0.43}$ icosahedron/C by electrochemical H insertion in PdH_x during HER.

DFT calculations

For face-centered cubic (fcc) Pd, the (111) plane is closely packed planes, and the exposed planes in icosahedral samples are also (111) planes. Therefore, Pd and PdH_x (111) surface are chosen as the representative surface in the following calculations.

1. Adsorption energy and Gibbs free energy

The adsorption energy ΔE_{ad} of hydrogen on Pd and PdH_x (111) surface is defined as

$$\Delta E_{\mathrm{ad}} = E_{\mathrm{surf+H^*}} - E_{\mathrm{surf}} - \frac{1}{2}E_{\mathrm{H_2}} \qquad (1)$$

where $E_{\mathrm{surf+H^*}}$, E_{surf}, and $E_{\mathrm{H_2}}$ are the total energies of the surface with H^* adsorption, clean surface, and hydrogen molecule in the gas phase, respectively.

The HER activity can be evaluated by $\Delta G_{\mathrm{H^*}}$, which is defined as

$$\Delta G_{\mathrm{H^*}} = \Delta E_{\mathrm{ad}} + \Delta E_{\mathrm{ZPE}} - T\Delta S_{\mathrm{H}} \qquad (2)$$

where ΔE_{ZPE} and ΔS_{H} are the difference in zero point energy and entropy between the adsorbed hydrogen and hydrogen in the gas phase, respectively, and T is 300 K. Herein, in

standard conditions, $\Delta E_{\mathrm{ZPE}} - T\Delta S_{\mathrm{H}}$ is approximated to be 0.24 eV.[13] Thus, Eqn. (2) can be simplified to

$$\Delta G_{\mathrm{H}^*} = \Delta E_{\mathrm{ad}} + 0.24\ \mathrm{eV} \qquad (3)$$

2. Computational models

For fcc Pd unit cell, different numbers of H atoms (1, 2, 3, and 4) are placed in the octahedral interstitial positions, which represent PdH_x with H concentrations of x = 0.25, 0.50, 0.75, and 1, respectively. The PdH_x (111) model used in the calculation is similar to the Pd-terminated β-PdH (111) model reported in previous literatures.[14] As shown in Figure S16, the Pd and PdH_x (111) surface is modeled as a 2×2 periodic slab with five Pd layers and is separated by a vacuum larger than 15 Å. Each Pd layer contains four Pd atoms. For PdH_x (111) surface, there is also one H layer between neighboring two Pd layers. The octahedral interstitial positions in the topmost subsurface (marked by red arrow) of PdH_x (111) surface (x<1.0) are artificially fully occupied by four H atoms in order to mimic the high H concentration in the subsurface compared to that in the PdH_x bulk. For the bottom three H layers (marked by black arrows), each H layer contains 1, 2, 3, and 4 H atoms for x=0.25, 0.50, 0.75, and 1, respectively. The surface is represented by the three topmost Pd and H layers, which are allowed to relax, while the other lower Pd and H layers are fixed to simulate the bulk layers.

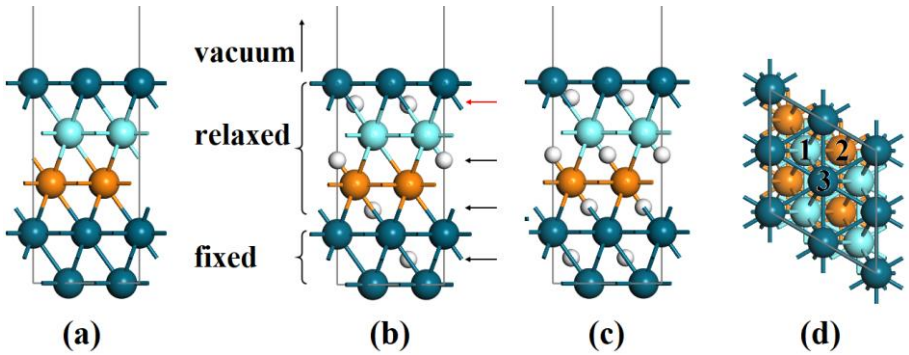

Figure S16 Side views of (a) Pd, (b) PdH0.25, and (c) PdH (111) surfaces. (d) Top view of Pd (111) surface and schematic illustration of the adsorption sites of H atom. The adsorption sites of 1 to 3 denote hcp, fcc, and top sites, respectively. The Pd atoms in the first, second, and third

Pd layers are represented as dark cyan, cyan, and orange spheres, respectively, and the H atom is represented as small white sphere.

The H atom is originally placed at high-symmetry site on Pd and PdH_x (111) surface, which corresponds to a coverage of 1/4 ML. There are three adsorption sites: hexagonal closed-packed (hcp), fcc, and top sites, which are schematically illustrated in Figure S16. The above adsorbed structures are fully relaxed to obtain the most favorable adsorption structures.

3. Adsorption on strained Pd (111) surface

For Pd (111) surface, the most favorable adsorption site for hydrogen atom is fcc site. The calculated ΔG_{H^*} on the fcc site of Pd (111) surface under tensile strain are plotted in Figure S17. The lattice parameters of Pd under the tensile strain ε of 1.4 %, 2.6 %, 3.6 %, and 4.5 % correspond to those of PdH_x with H concentrations of x = 0.25, 0.50, 0.75, and 1, respectively. The unstrained Pd (111) surface shows strong adsorption of hydrogen atom with ΔG_{H^*} of -0.459 eV. Furthermore, it can be seen that the $|\Delta G_{H^*}|$for Pd (111) surface gradually increases as the increase of the tensile strain, indicating that the adsorption of hydrogen atom is further strengthened. Therefore, the expansion of Pd lattice under the tensile strain is not benefit to the HER activity.

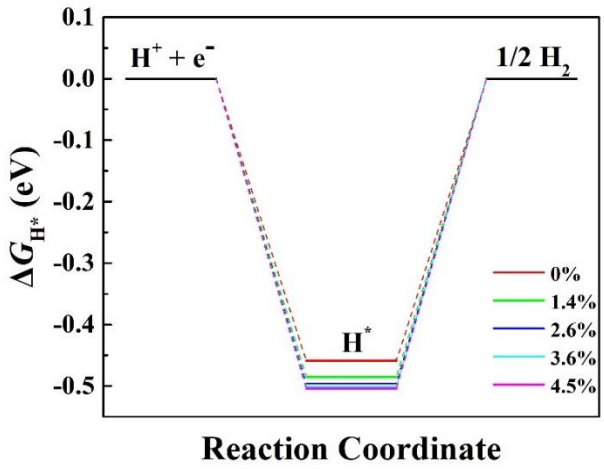

Figure S17 The calculated ΔG_{H^*} for hydrogen adsorption on Pd (111) surface under a series of tensile strain.

References

1. T. Lv, Y. Wang, S.-I. Choi, M. Chi, J. Tao, L. Pan, C. Z. Huang, Y. Zhu and Y. Xia, *ChemSusChem*, 2013, **6**(10), 1923.
2. M. Jin, H. Zhang, Z. Xie and Y. Xia, *Energy Environ. Sci.*, 2012, **5**(4), 6352.
3. Z. Zhao, X. Huang, M. Li, G. Wang, C. Lee, E. Zhu, X. Duan and Y. Huang, *J. Am. Chem. Soc.*, 2015, **137**(50), 15672.
4. H. Liao, C. Wei, J. Wang, A. Fisher, T. Sritharan, Z. Feng and Z. J. Xu, *Adv. Energy Mater.*, 2017, **7**(21), 1701129.
5. Y. Liu, J. Wu, K. P. Hackenberg, J. Zhang, Y. M. Wang, Y. Yang, K. Keyshar, J. Gu, T. Ogitsu, R. Vajtai, J. Lou, P. M. Ajayan, Brandon C. Wood and B. I. Yakobson, *Nature Energy*, 2017, **2**(9), 17127.
6. H. Lv, X. Chen, D. Xu, Y. Hu, H. Zheng, S. L. Suib and B. Liu, *Applied Catalysis B: Environmental*, 2018, **238**, 525.
7. X. Zhang, D. Wu and D. Cheng, *Electrochim. Acta*, 2017, **246**, 572.
8. M. D. Segall, P. J. D. Lindan, M. J. Probert, C. J. Pickard, P. J. Hasnip, S. J. Clark and M. C. Payne, *J. Phys.: Condens. Matter*, 2002, **14**(11), 2717.
9. J. P. Perdew, K. Burke and M. Ernzerhof, *Phys. Rev. Lett.*, 1996, **77**(18), 3865.
10. D. Vanderbilt, *Phys. Rev. B*, 1990, **41**(11), 7892.
11. H. J. Monkhorst and J. D. Pack, *Phys. Rev. B*, 1976, **13**(12), 5188.
12. A. Tkatchenko and M. Scheffler, *Phys. Rev. Lett.*, 2009, **102**(7), 073005.
13. J. K. Nørskov, T. Bligaard, A. Logadottir, J. R. Kitchin, J. G. Chen, S. Pandelov and U. Stimming, *J. Electrochem. Soc.*, 2005, **152**(3), J23.
14. M. P. Jigato, B. Coussens and D. A. King, *The Journal of Chemical Physics*, 2003, **118**(12), 5623.